F-actin polymerization and retrograde flow drive sustained PLCγ1 signaling during T cell activation

Alexander Babich,[1,3] Shuixing Li,[1,2] Roddy S. O'Connor,[1,3] Michael C. Milone,[1,3] Bruce D. Freedman,[4] and Janis K. Burkhardt[1,2,3]

[1]Department of Pathology and Laboratory Medicine, [2]Children's Hospital of Philadelphia, and [3]Perelman School of Medicine, University of Pennsylvania, Philadelphia, PA 19104
[4]Department of Pathobiology, University of Pennsylvania School of Veterinary Medicine, Philadelphia, PA 19104

Activation of T cells by antigen-presenting cells involves assembly of signaling molecules into dynamic microclusters (MCs) within a specialized membrane domain termed the immunological synapse (IS). Actin and myosin IIA localize to the IS, and depletion of F-actin abrogates MC movement and T cell activation. However, the mechanisms that coordinate actomyosin dynamics and T cell receptor signaling are poorly understood. Using pharmacological inhibitors that perturb individual aspects of actomyosin dynamics without disassembling the network, we demonstrate that F-actin polymerization is the primary driver of actin retrograde flow, whereas myosin IIA promotes long-term integrity of the IS. Disruption of F-actin retrograde flow, but not myosin IIA contraction, arrested MC centralization and inhibited sustained Ca^{2+} signaling at the level of endoplasmic reticulum store release. Furthermore, perturbation of retrograde flow inhibited PLCγ1 phosphorylation within MCs but left Zap70 activity intact. These studies highlight the importance of ongoing actin polymerization as a central driver of actomyosin retrograde flow, MC centralization, and sustained Ca^{2+} signaling.

Introduction

T cell activation by antigen-presenting cells (APCs) requires the formation of a specialized cell–cell interface, known as the immunological synapse (IS). This process involves extensive spatial and temporal regulation of protein complexes to coordinate and tune signaling events. Initial T cell receptor (TCR) engagement triggers the formation of submicrometer-scale signaling microclusters (MCs) enriched in receptors, kinases, and adaptor proteins that propagate downstream signaling events. In the MCs, the Src kinase Lck phosphorylates the ζ chains of the TCR complex. ζ-Chain–associated protein of 70 kD (Zap70), a kinase crucial in MC assembly, associates with TCR and phosphorylates LAT (linker of activated T cells) and SH2 domain–containing leukocyte protein of 76 kD (SLP-76). Cooperative assembly of these and other MC components culminates in the recruitment and subsequent activation of phospholipase C (PLC) γ1 at the plasma membrane (Houtman et al., 2004; Bunnell et al., 2006; Sherman et al., 2011). Upon activation, PLCγ1 cleaves PIP_2 into diacylglycerol and inositol 1,4,5-trisphosphate (IP_3). Subsequently, IP_3 stimulates the release of Ca^{2+} from ER stores, which in turn leads to the opening of Orai1 channels in the plasma membrane (Zhang et al., 1999). The resulting sustained Ca^{2+} signaling is required for initiation of gene transcription.

Newly generated MCs arise in the periphery of the IS and are the predominant sites for active signaling (Bunnell et al., 2002; Lee et al., 2002; Yokosuka et al., 2005). These structures undergo continuous translocation to the center of the IS, the central supramolecular activation cluster (cSMAC), where signaling is extinguished. This provides a clock for MC lifetime and is thought to modulate antigen response (Valitutti et al., 2010). MC dynamics are dependent on the actin cytoskeleton in complex ways. Treatment of spreading T cells with the F-actin depolymerizing agent latrunculin A inhibits formation of new MCs, indicating that actin filaments promote MC assembly. Once formed, however, MCs are stable in the absence of F-actin, although their

Correspondence to Janis K. Burkhardt: jburkhar@mail.med.upenn.edu

Abbreviations used in this paper: APC, antigen-presenting cell; CB, cell body; CRAC, calcium release–activated calcium; cSMAC, central supramolecular activation cluster; GAPDH, glyceraldehyde 3-phosphate dehydrogenase; IS, immunological synapse; LM, lamellum; LP, lamellipodium; MC, microcluster; MLC, myosin light chain; PLC, phospholipase C; TCR, T cell receptor; Tg, thapsigargin.

The Rockefeller University Press $30.00
J. Cell Biol. Vol. 197 No. 6 775–787
www.jcb.org/cgi/doi/10.1083/jcb.201201018

centripetal movement ceases upon F-actin depletion. In keeping with the close association between signaling MCs and the actin cytoskeleton, T cell activation is highly dependent on maintenance of an intact F-actin network. Treatment of T cells with actin depolymerizing agents or disruption of key actin regulatory proteins leads to loss of Ca^{2+} mobilization and downstream transcriptional activation (Nolz et al., 2006; Varma et al., 2006).

Recent studies have shown that TCR-induced F-actin polymerization depends on activation of the Arp2/3 complex by multiple nucleation-promoting factors, including WAVE2, HS1, and Wiskott–Aldrich syndrome protein (Zhang et al., 1999; Gomez et al., 2006; Nolz et al., 2006). However, the mechanisms that coordinate F-actin retrograde flow and disassembly of the F-actin network are largely unexplored, and the role of myosin II contractility is poorly understood and controversial. Jacobelli et al. (2004) showed that nonmuscle myosin IIA is recruited to the IS but found that activity of this motor protein was dispensable for conjugate formation and for recruitment of signaling molecules to the IS. In contrast, Ilani et al. (2009) found that inhibition or knockdown of myosin IIA disrupts T cell–APC conjugates and inhibits multiple aspects of TCR signaling. In that study, centripetal TCR MC movement was shown to be myosin II dependent. As myosin II contractility is known to contribute to actin retrograde flow in nonhematopoietic cells (Cai et al., 2006), this could reflect a linkage between myosin II function, F-actin retrograde flow, and MC centralization. Understanding this process will require detailed analysis of actomyosin dynamics with respect to distinct MC components.

The mechanisms that link the actin cytoskeleton to T cell signaling in general are largely unknown. F-actin could promote signaling in multiple ways, including maintaining cell–cell contact, organizing gross cell polarity, and providing a nanoscale scaffold for assembly of signaling complexes (Wülfing and Davis, 1998; Kaizuka et al., 2007). Recent studies also point to the exciting possibility that F-actin dynamics could actively promote signaling by exerting force on receptors or signaling molecules (Alon and Dustin, 2007; Beemiller and Krummel, 2010). These possibilities are not mutually exclusive but cannot be distinguished based on manipulations that globally deplete actin filaments.

In this study, we have systematically studied the roles of actin polymerization and myosin II contractility in controlling protein dynamics and signaling during T cell activation. We find that F-actin and myosin IIA exhibit distinct but overlapping distributions at the IS. Using a panel of cytoskeletal inhibitors together with an RNAi approach, we find that actin polymerization is the primary driver of actomyosin retrograde flow, whereas myosin IIA exerts contractile forces on the network and helps maintain its radial symmetry. We show that simultaneous inhibition of both F-actin turnover and myosin IIA contractility leads to arrest of retrograde flow without disassembling the actin network. Under these conditions, centralization of SLP-76 MCs is also arrested, and Ca^{2+} elevation is abrogated at the level of release from stores. PLCγ1 phosphorylation is inhibited after F-actin immobilization, but Zap70 remains active, showing that cytoskeletal dynamics selectively affect specific signaling molecules at the IS. Our studies demonstrate a requirement for F-actin dynamics, rather than a static F-actin scaffold, in promoting T cell activation.

Results

Quantitative analysis of actomyosin flow at the IS

Numerous studies have shown the importance of actin for T cell activation, but the mechanics of actin movement at the IS have not been carefully addressed. Moreover, myosin II function at the IS is poorly understood, and results are conflicting (Jacobelli et al., 2004; Ilani et al., 2009). To investigate the actomyosin network as a functional unit, we used Jurkat T cells stably expressing low levels of GFP-actin (Gomez et al., 2006) and transfected with mKate2-tagged heavy chain of nonmuscle myosin IIA (NMHC II-A). When these cells were allowed to spread on anti-CD3–coated coverglasses, they formed characteristic actin-rich lamellipodial protrusions. Consistent with previous observations (Bunnell et al., 2001; Gomez et al., 2006), cell spreading reached a maximum within 2–4 min and was maintained for 15–20 min before partial contraction. We concentrated our studies on the fully spread cells, representing the sustained phase of TCR signaling. Myosin IIA localized to the IS (Fig. 1 A), as reported previously in T cell–APC conjugates (Jacobelli et al., 2004). Intensity profile analysis showed that myosin IIA was present throughout the actin-rich region but accumulated most prominently behind the lamellipodium (LP; Fig. 1 B). Importantly, although the distribution of F-actin and myosin IIA are distinct, they are overlapping; F-actin was detectable throughout the myosin-rich region, albeit at lower levels than in the LP. Indeed, the presence of myosin IIA within the lamellum (LM) region highlights a pool of F-actin that is not readily appreciated in images contrasted for optimal observation of the more abundant actin filaments in the LP. Similar distributions were observed using antibody and phalloidin labeling of endogenous myosin IIA and F-actin in fixed cells (Fig. 1 D; also see Fig. 3 E).

Live-cell microscopy revealed that myosin IIA undergoes continuous retrograde flow comparable with that of F-actin (Video 1). During its centripetal movement, myosin IIA became organized into prominent bundles, and actin was present in these structures (unpublished data). Interestingly, both actin and myosin IIA were nearly undetectable in the central region of the IS. This was not a result of an artifact of cell shape and shallow focal plane, as 3D reconstructions showed that the network exhibits a planar organization only ∼1 µm in thickness. We could readily detect other structures within this region (e.g., SLP-76 MCs in Fig. 1 D and the microtubule-organizing center [not depicted]). Based on these studies, we define three regions with distinct cytoskeletal topology: the actin-rich LP, the myosin IIA–rich LM, and the cell body (CB), a perinuclear region largely devoid of actomyosin filaments.

Next, we quantified the velocity of the F-actin retrograde flow in two complementary ways. First, videos were digitally sharpened to amplify signal-to-noise, and fiduciary features with ∼1–2-µm spacing along the radius were tracked

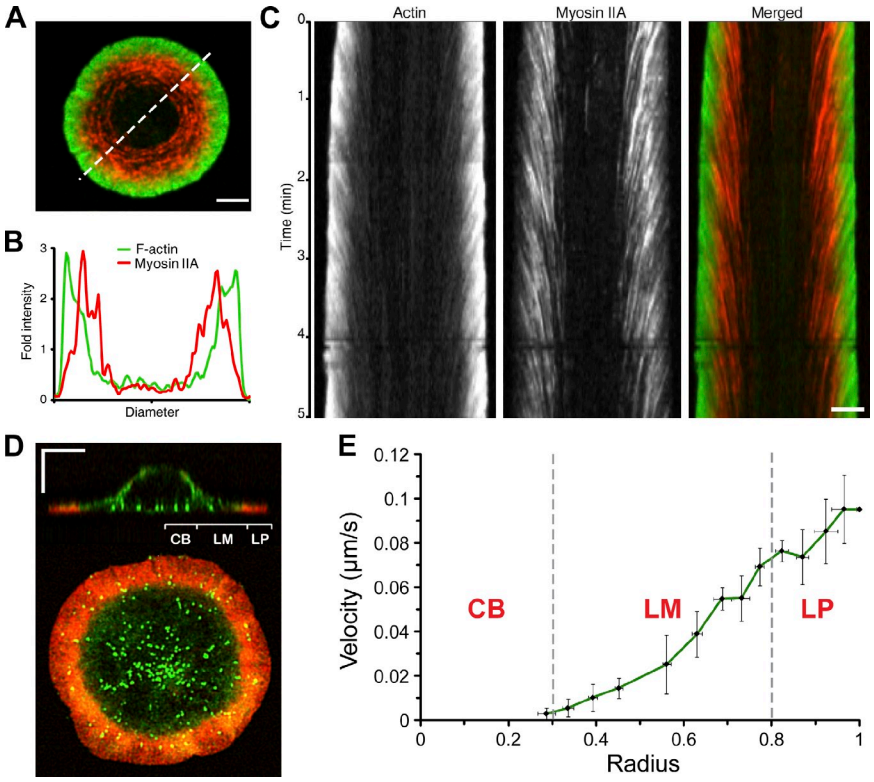

Figure 1. **Distribution and dynamics of the T cell actomyosin network.** (A) mKate2–NMHC II-A was transiently expressed in Jurkat T cells stably expressing GFP-actin. The cells were dropped on OKT3-coated coverglasses and imaged at a single focal plane every 3 s (also see Video 1). An image from a sequence is shown and is representative of four independent experiments. Bar, 5 µm. (B) The intensity profile of F-actin and myosin IIA was acquired along the dashed line in A. (C) A composite kymograph of actomyosin dynamics was acquired along the dashed line in A. Bar, 5 µm. (D) Jurkat T cells stably expressing GFP–SLP-76 (green) were stimulated as in A, fixed after 5 min, and stained for F-actin with phalloidin (red). Z stacks of whole cells were collected with a 0.25-µm step size and deconvolved using a calculated Point Spread Function in Volocity. A representative cell is shown in XZ and XY planes. Brackets represent 5 µm × 5 µm. (E) Kymographic analysis of F-actin features was compiled into a single graph to show the distribution of F-actin velocity across the IS radius. Mean ± SD is shown for each point (n = 13 cells). Similar results were obtained from three independent experiments.

by kymography (Fig. S1 [A and B] and Video 2). Alternatively, a region was photobleached to induce synchronous incorporation of bleached GFP-actin into the network, generating a high-contrast wave that is easily identified by kymography (Fig. S1 C and Video 3). Results using both approaches were in agreement and showed that F-actin flow within the LP proceeds at 0.095 ± 0.028 µm/s. Upon closer examination of these kymographs, however, we noted that actin velocity depended on position along the radius of the IS. This is evident in Fig. S1 B, where the slope of the red line drawn near the periphery of the IS is shallower than that of the blue line drawn in the LM region, indicating a slowing of movement toward the IS center. Features within the central CB region track vertically (yellow line in Fig. S1 B), indicating that they are immobile. Similar behavior is evident in kymographs generated from myosin IIA videos (Fig. 1 C). The distribution of actomyosin dynamics across the IS in a population of cells is shown in Fig. 1 E, with the three regions of the IS indicated for comparison. Centripetal flow decelerates gradually from the periphery through the LM. The occasional features that show movement within the CB region appear to be diffusive.

Myosin IIA exerts contractile force on the F-actin network but is dispensable for F-actin flow

The observed centripetal flow could be driven by F-actin polymerization pushing against the membrane edge (Pollard and Berro, 2009) or myosin II contraction pulling against the branched F-actin network (Cai et al., 2006; Wilson et al., 2010). To uncouple these components, we used a panel of well-defined pharmacological inhibitors. Initially, we tested the effects of jasplakinolide (JAS), an F-actin stabilizing agent that perturbs actin turnover (Bubb et al., 1994). T cells pretreated with JAS were not useful for analysis, as this abrogated cell spreading and induced cytoplasmic F-actin aggregates (unpublished data). Therefore, we allowed cells to contact a stimulatory coverglass for 3 min before addition of the drug. Acute addition of JAS collapsed the F-actin network toward the center of the IS. This was true in both Jurkat T cells (Fig. 2 A and Video 4 [left]) and human primary T cell blasts (Fig. 2 B and Video 5). Myosin IIA (Fig. 2 C and Video 4 [right]) behaved similarly, with two important differences. First, the collapse of myosin IIA was more rapid. This is evident in the kymographic analysis of F-actin and myosin IIA dynamics (Fig. 2, D and E, respectively). Second, unlike F-actin, which accumulated in an irregular ring around the CB, myosin IIA transiently formed a tight symmetrical ring that subsequently disappeared as large aggregates accumulated in the periphery. Thus, myosin IIA exerts centripetal force on the T cell cytoskeleton, which is revealed upon stabilization of the F-actin network.

Next, we analyzed retrograde flow under conditions in which myosin II activity is perturbed. The Rho kinase inhibitor Y-27632 blocks phosphorylation of myosin light chain (MLC) at S19 and inhibits myosin II filament assembly (Ueda et al., 2002). Surprisingly, T cells pretreated with Y-27632 continued to show retrograde F-actin flow with unchanged rate (Fig. 3 [A and B] and Video 6). The drug successfully inhibited MLC phosphorylation, based on immunoblotting using a phospho-specific antibody (Fig. 3 B, bottom). As a more direct test of myosin II function, we generated Jurkat T cells expressing the F-actin sensor F-tractin labeled with tdTomato (Johnson and Schell, 2009) and measured actin dynamics in cells treated

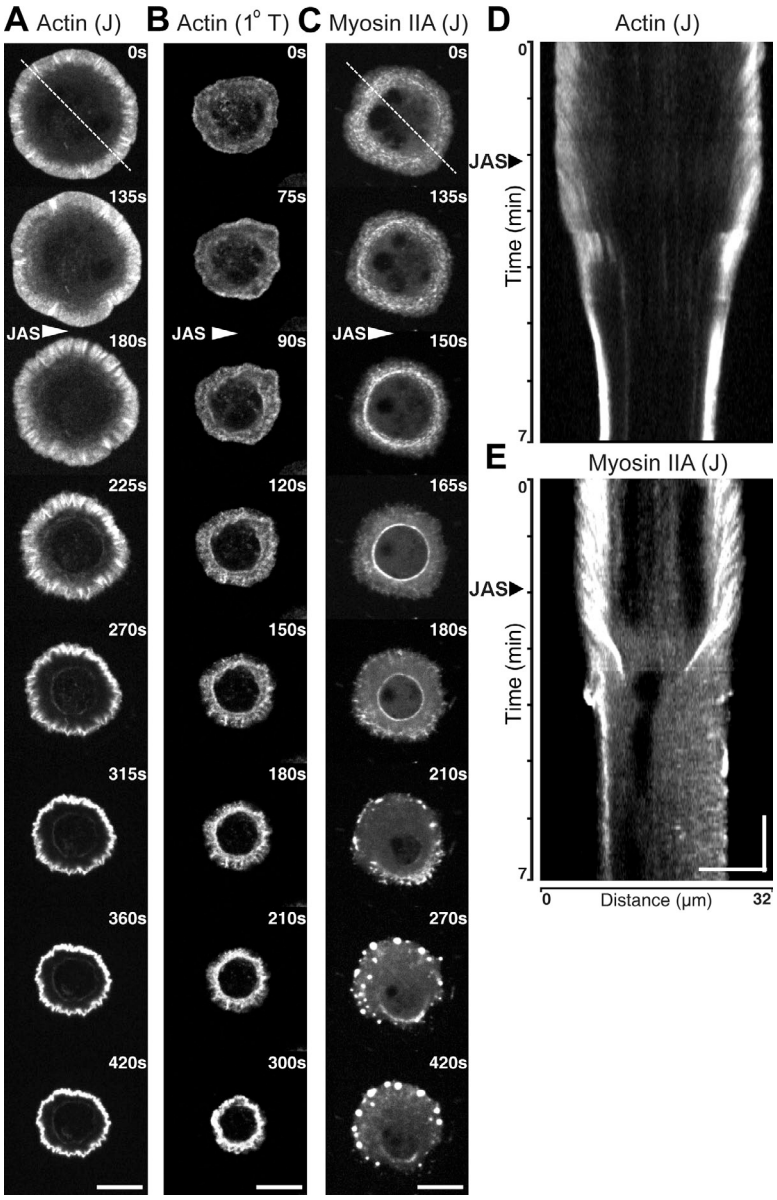

Figure 2. **F-actin stabilization leads to contraction of the actomyosin network.** (A–C) Time-lapse series of T cells spreading on OKT3-coated coverslips. Arrowheads indicate times when 1 µM JAS was added. Bars, 10 µm. (A) Jurkat T cells stably expressing GFP-actin (see Video 4). (B) Primary human T cell blasts transiently transfected with GFP-actin (see Video 5). (C) E6.1 Jurkat T cells transiently transfected with GFP–NMHC IIA (see Video 6). (D and E) Kymographs of F-actin and myosin dynamics, generated along the dashed lines in A and C, respectively. Arrowheads indicate the addition of 1 µM JAS into the media. Brackets represent 10 µm × 1 min.

with blebbistatin, a specific inhibitor of myosin II ATPase activity (Straight et al., 2003). As shown in part A of Video 7 and quantified in Fig. 3 C, the rates of retrograde flow were unaffected by blebbistatin pretreatment. Finally, siRNA was used to suppress expression of myosin IIA heavy chain (Myh9). We could suppress protein levels by 75% without any effect on the rate of actin retrograde flow (Fig. 3 D). Taken together with the aforementioned results, these studies show that myosin II exerts contractile forces on the T cell actin network, but these forces are dispensable for actin retrograde flow at the IS.

T cells responding to ligand-coated surfaces exhibit initial expansion of the contact area, a steady-state period during which the area remains constant, and a contraction phase. Time-course analysis of IS organization showed that control and myosin-inhibited cells looked comparable during the expansion and steady-state phases of the response. After 10–15 min, however, myosin-inhibited cells failed to contract normally and became irregularly shaped (Fig. 3, E and F). Moreover, the F-actin network looked thinner and more disorganized. Thus, although myosin II activity is dispensable for F-actin flow, it limits cell spreading and maintains synaptic integrity over time.

Inhibition of myosin IIA and F-actin turnover arrests cytoskeletal retrograde flow

Having analyzed F-actin and myosin II inhibitors separately, we next evaluated their cumulative effect on cytoskeletal dynamics. T cells were pretreated with Y-27632 and allowed to interact with the TCR-stimulatory surface to allow spreading. JAS was then added to the chamber, resulting in arrest of F-actin retrograde flow within ∼30 s (Fig. 4 A and Video 8 [part A]). The frozen network persisted for several minutes but then thinned and eventually dissipated (unpublished data). To verify the complete lack of dynamics, we bleached a region within the LP. Cells treated with Y-27632 and JAS showed no fluorescence recovery, whereas

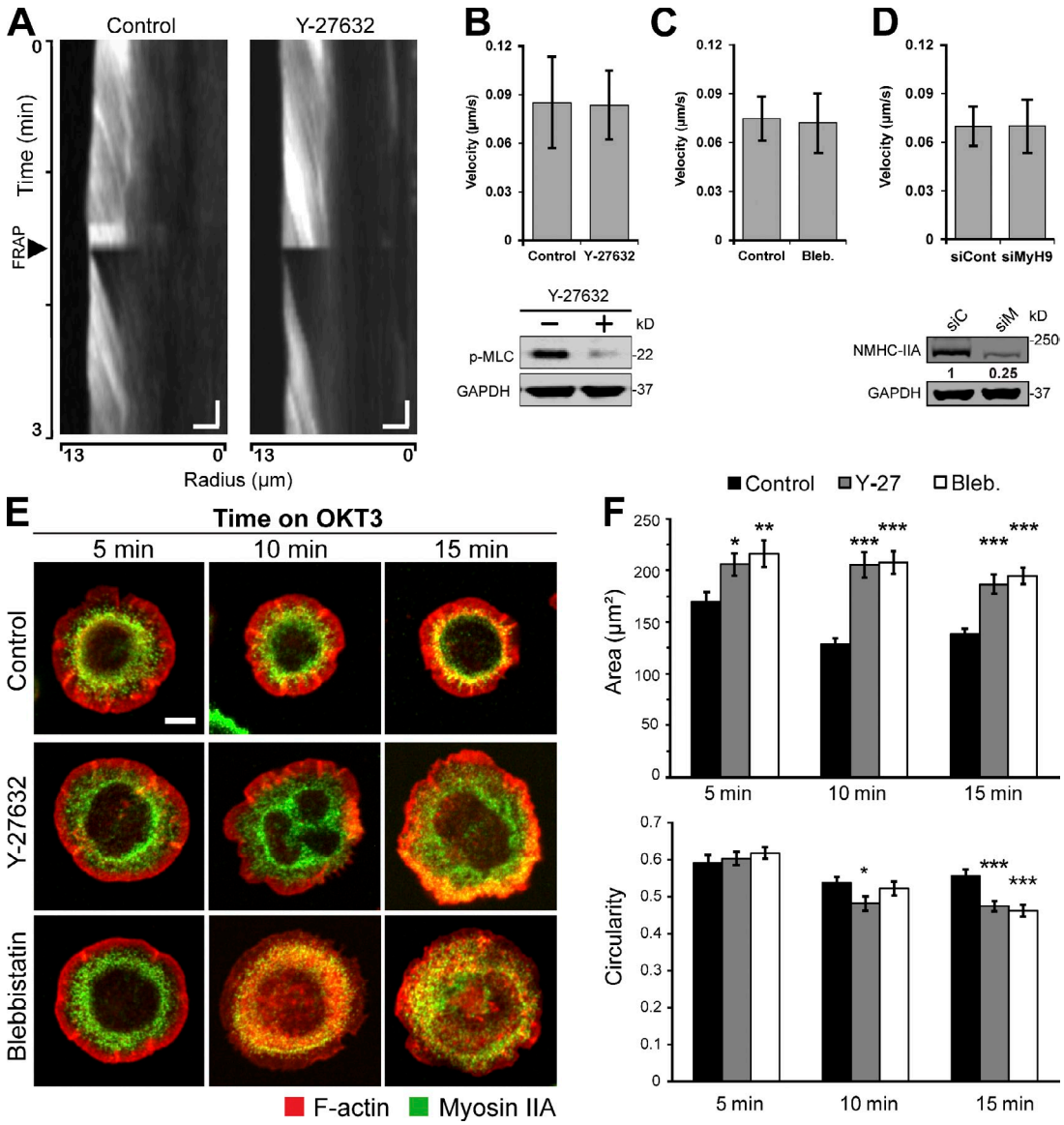

Figure 3. **Myosin IIA is not required for F-actin flow but is necessary for long-term maintenance of the IS.** (A) GFP-actin–expressing Jurkat T cells were pretreated for 15 min with vehicle or 25 µM Y-27632 and imaged while spreading on anti-CD3–coated coverslips. Kymographs were generated along the radii of fully spread cells. The arrowhead indicates the time when photobleaching of lamellipodia was induced. Brackets represent 2 µm × 15 s. (B, top) Analysis of velocities calculated from kymographs as in A (mean ± SD, *n* = 15 cells). (bottom) To verify inhibitory activity of Y-27632, Jurkat T cells were pretreated with Y-27632 as in A and stimulated with OKT3 (1 µg/ml) for 5 min. Cells were lysed and analyzed by Western blot analysis with antibodies to phosphorylated MLC (pMLC) or GAPDH. (C) Jurkat T cells were transiently transfected with F-tractin tdTomato and pretreated with 50 µM blebbistatin (Bleb.) or vehicle for 30 min. Actin retrograde flow was analyzed as in B. Values are mean ± SD of 80–90 kymographs from 14–20 cells. (D) GFP-actin–expressing Jurkat T cells were transfected with oligonucleotides specific for myosin IIA heavy chain (SiM) or control oligonucleotides (SiC) and cultured for 48 h, at which time suppression was found to be optimal. (top) Retrograde flow was analyzed as in B. (bottom) Lysates were analyzed by Western blotting to assess efficiency of suppression. Values represent relative NMHC II-A levels, normalized to GAPDH. (E) Jurkat T cells were untreated or pretreated with 25 µM Y-27632 or 50 µM blebbistatin and allowed to spread for the indicated times on anti-CD3–coated coverslips before fixation and labeling with phalloidin and anti–NMHC II-A. Bar, 5 µm. (F) Morphometric analysis of cells prepared as in E. Data represent mean ± SEM (*n* = 67–125 cells per condition). *, P < 0.05; **, P < 0.01; ***, P < 0.001. Similar results were obtained in two independent experiments.

control cells recovered normally (Fig. 4 B). Similar results were observed in primary T cell blasts treated with Y-27632 and JAS (Video 8, part B) and in Jurkat T cells treated with blebbistatin and JAS (not depicted). In T cells suppressed for myosin IIA, JAS treatment did not result in complete loss of actin dynamics; instead, a slow, partial collapse of the actin network was observed (Fig. S2 A and Video 7 [part B]). This may reflect the activity of residual myosin IIA or the function of myosin IIB, which is also expressed in these cells (Fig. S2 B). Collectively, these studies show that actin polymerization is the primary engine for retrograde F-actin flow in T cells. Continuous F-actin flow is driven by ongoing assembly of actin filaments in the LP, coupled to disassembly in the LM, with overall organization provided by myosin II.

F-actin retrograde flow governs SLP-76 MC centralization

The mechanisms linking MC movement and signaling to F-actin dynamics are poorly understood. Furthermore, recent studies

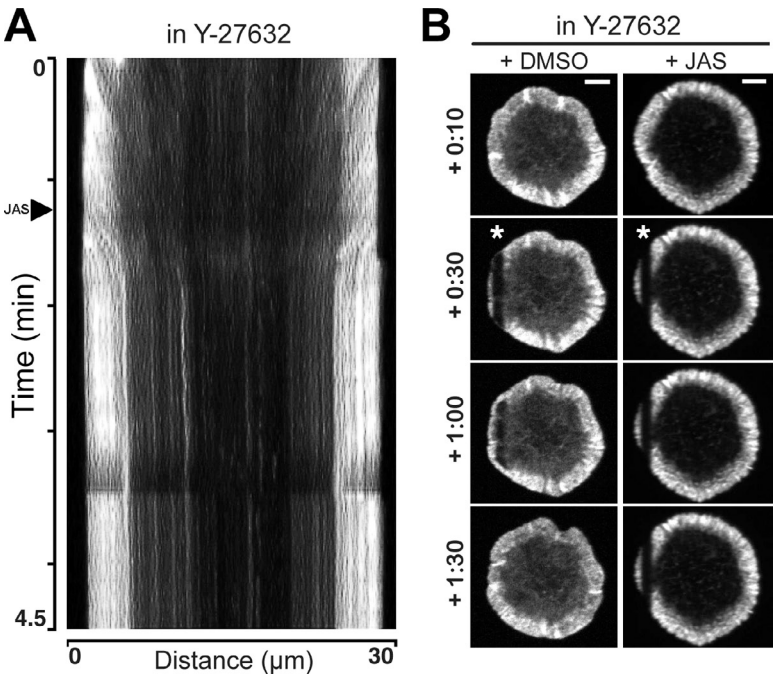

Figure 4. **Inhibition of myosin IIA and F-actin stabilization arrests retrograde flow.** (A) A kymograph was generated along the diameter of a cell pretreated with 25 µM Y-27632 and spreading on OKT3-coated coverglasses. The arrowhead along the time axis indicates the addition of 1 µM JAS to the well. The kymograph was sharpened in Photoshop to accentuate F-actin features. (B) Time-lapse series of cells pretreated with 25 µM Y-27632 and allowed to interact with the stimulatory surface for 5 min before addition of either DMSO or 1 µM JAS. 30 s after the treatment, a portion of F-actin, marked with an asterisk, was photobleached, and fluorescence recovery was recorded. Bars, 5 µm.

show that microtubules can direct MC movement (Bunnell et al., 2002; Lasserre et al., 2010; Hashimoto-Tane et al., 2011). We took advantage of our ability to manipulate actin flow to examine the relationship between the actomyosin network and SLP-76 MC dynamics. As we were unsuccessful in raising a stable cell line expressing fluorescently tagged actin and SLP-76, we imaged a mixture of GFP–SLP-76 and GFP-actin T cells to conduct side-by-side analysis of these proteins in response to pharmacological intervention. As expected, treatment with Y-27632 did not perturb F-actin flow (Fig. 5 A, before arrowhead). SLP-76 MCs also continued to centralize normally in the presence of Y-27632, indicating that myosin II activity is dispensable for their dynamics (Fig. 5 B). After addition of JAS, however, MC centralization was arrested concomitantly with the arrest of F-actin (Fig. 5 A [after arrowhead] and Video 9). Interestingly, even MCs close to the center, where F-actin was sparse, stopped their movement. This result is also shown in maximum-over-time projections of video sequences (Fig. 5 C). In these images, moving SLP-76 MCs, seen as radial streaks, are readily apparent in cells treated with Y-27632 alone, but only stationary SLP-76 MCs, visible as spots, are evident after the addition of JAS to freeze the F-actin network. Finally, it is important to note that no new MCs formed in the absence of F-actin retrograde flow (unpublished data). Collectively, these observations suggest that dynamic F-actin, and not simply F-actin accumulation at the IS, is required for SLP-76 MC nucleation and centripetal movement.

SLP-76 MC dynamics do not correlate with F-actin behavior

Qualitatively, SLP-76 MC centralization did not resemble actomyosin movement (e.g., MCs often gathered at the center of the IS, where little F-actin was present to facilitate their movement; Fig. S3 A and Video 10). Therefore, we performed careful quantitative measurements of MC velocity to seek clues to the driving mechanism. Particle tracking and kymographic analysis yielded very similar results. Both techniques revealed that SLP-76 MCs centralized with relatively constant velocity, averaging 0.065 ± 0.059 µm/s based on particle tracking and 0.059 ± 0.034 µm/s based on kymography (Fig. S3). This differs dramatically from the behavior of F-actin, which decelerated with inward movement. F-actin and SLP-76 MC centripetal velocity distributions are overlaid in Fig. 5 D. From this analysis, it is evident that although F-actin retrograde flow could drive SLP-76 MC movement in the periphery of the IS, SLP-76 MCs actually move faster than the actin network in the LM and CB regions. Thus, a second mechanism is needed to account for MC dynamics in these regions.

F-actin dynamics are necessary for sustained Ca^{2+} signaling

Retention of MCs in the IS periphery by integrin ligands, genetic perturbations, or physical barriers correlates with enhanced T cell activation (Mossman et al., 2005; Nguyen et al., 2008; Hashimoto-Tane et al., 2011). To assess the effect of MC arrest in the context of F-actin immobilization, we first examined the effects on sustained Ca^{2+} entry, a hallmark of T cell activation (Negulescu et al., 1994; Oh-hora, 2009). Cells were loaded with the ratiometric dye fura-2 acetoxymethyl ester and imaged while settling on stimulatory coverslips (Fig. 6 A). Despite previous reports that myosin IIA contractility is essential for Ca^{2+} entry (Ilani et al., 2009), we found no difference in Ca^{2+} mobilization in cells pretreated with Y-27632 and control cells. Both showed a rapid increase in intracellular Ca^{2+}, with levels declining gradually over the next 15–30 min. To assess the freeze condition, we pretreated cells with Y-27632 and allowed them to spread on OKT3 for 5 min before application of JAS (Fig. 6 B, red line). Intracellular Ca^{2+} levels began to drop

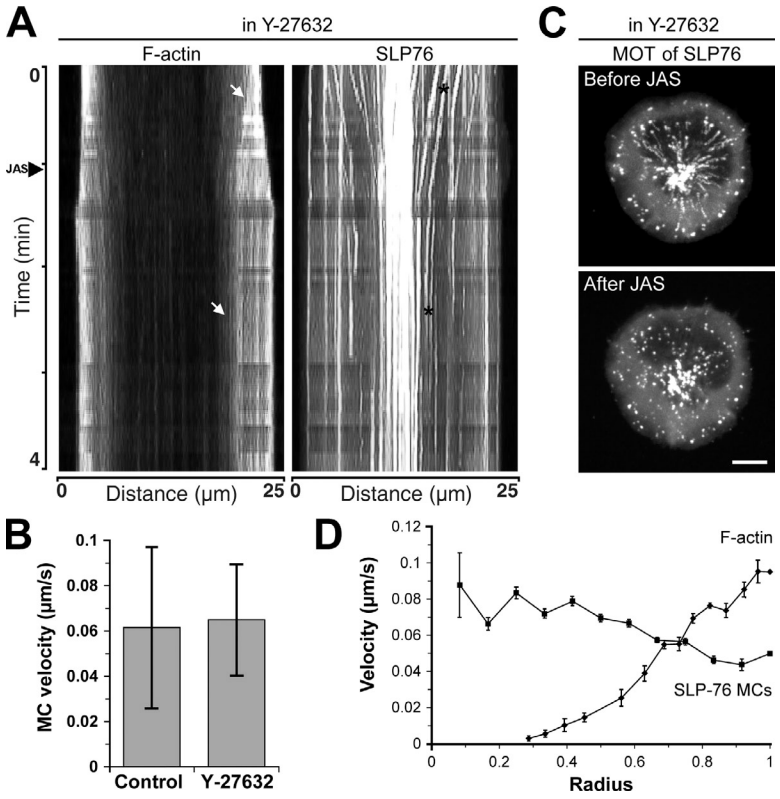

Figure 5. **F-actin governs MC dynamics but has different velocity distribution across the IS.** (A) Kymographs were generated along the diameter of cells expressing GFP-actin and GFP–SLP-76 and sharpened in Photoshop as in Fig. S1 B. The arrowhead along the time axis indicates the addition of 1 μM JAS. Arrows in the kymograph of F-actin dynamics point to a feature that became immobilized upon addition of JAS. Asterisks in the kymograph of SLP-76 dynamics indicate an MC that was immobilized by addition of JAS. (B) Jurkat T cells expressing GFP–SLP-76 were pretreated with either vehicle control or Y-27632 and allowed to spread on OKT3-coated coverglasses. Velocities of SLP-76 MCs were analyzed by kymography (mean ± SD, n = 40–150 MCs from 10–19 cells). (C) Maximum-over-time (MOT) images of GFP–SLP-76 Jurkat T cells were compiled from the images acquired before or after the addition of JAS. Images are representative of three independent experiments. Bar, 10 μm. (D) Comparative analysis of SLP-76 MC centripetal velocity from a single cell overlaid with F-actin dynamics from Fig. 1 E. Mean ± SEM is shown.

within 30 s of JAS addition, roughly the same lag period observed for F-actin arrest (Fig. 4 A). Within 3 min, Ca^{2+} had diminished to baseline levels, as defined by cells interacting with poly-L-lysine alone. A similar loss of sustained intracellular Ca^{2+} was observed when cells were treated with JAS alone (Fig. 6 B, green line), indicating that F-actin turnover is essential for sustained Ca^{2+} signaling.

Loss of intracellular Ca^{2+} could result from changes in Ca^{2+} release from ER stores or from inhibition of Ca^{2+} entry through calcium release–activated calcium (CRAC) channels in the plasma membrane. To test whether the defect was at the level of ER store release, we treated cells with either JAS alone (Fig. 6 C) or Y-27632 + JAS (Fig. 6 D) to inhibit Ca^{2+} signaling and then added the sarco/ER Ca^{2+}-ATPase pump inhibitor

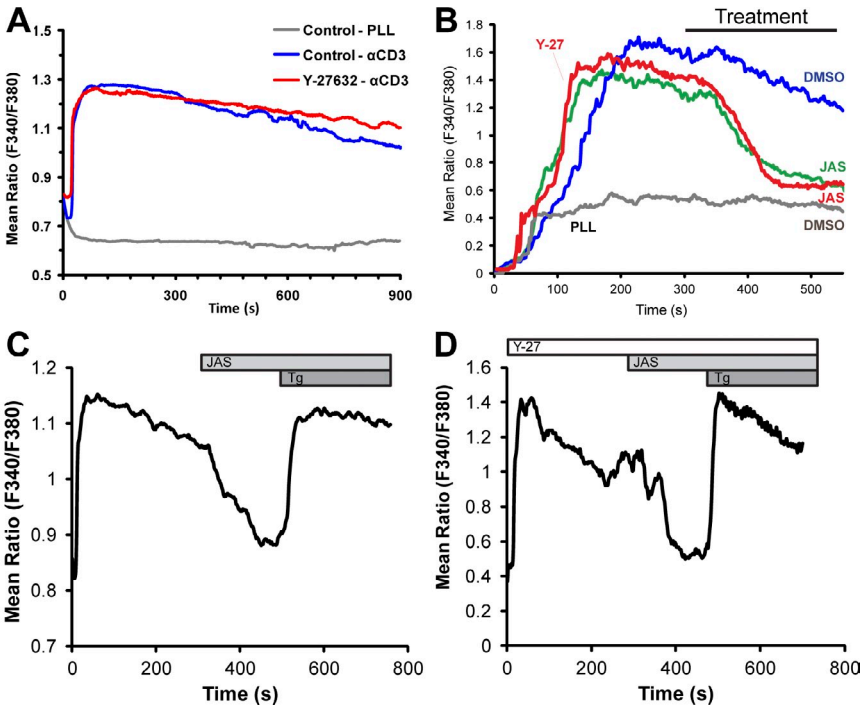

Figure 6. **Loss of F-actin dynamics abrogates sustained Ca^{2+} signaling by perturbing Ca^{2+} release from ER stores.** (A) GFP-actin Jurkat T cells were pretreated with 25 μM Y-27632 or left untreated and loaded with fura-2 before plating on OKT3- or poly-L-lysine (PLL)–coated coverglasses in 2 mM Ca^{2+}. (B) Cells were pretreated as in A and allowed to interact with the stimulatory surfaces for 5 min. DMSO or JAS was then added to the imaging chamber, and the response was measured for another 5 min. Similar results were obtained from three independent experiments. (C and D) Cells were pretreated as in B. 1 μM Tg was added to the dishes to induce Ca^{2+} release from ER stores.

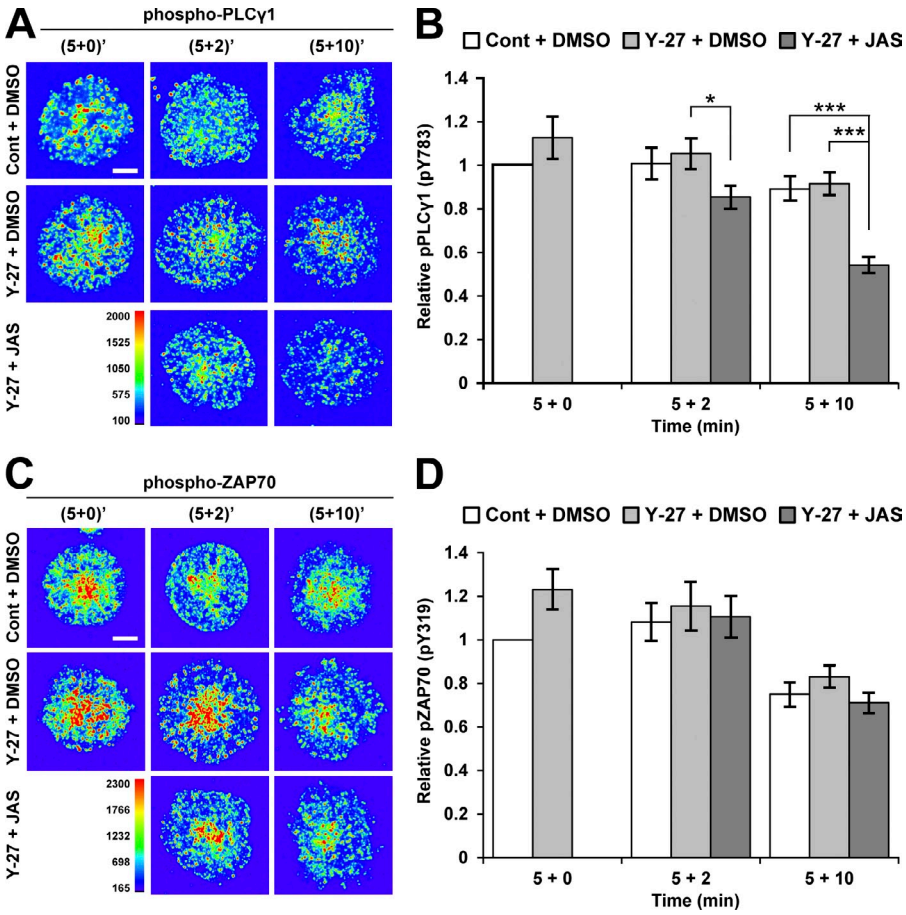

Figure 7. **F-actin immobilization selectively inhibits PLCγ1 phosphorylation.** (A and C) GFP-actin Jurkat T cells were either pretreated with 25 µM Y-27632 (Y-27) or left untreated and plated on OKT3-coated coverglasses. After 5 min, cells were treated with DMSO or JAS, then fixed at the indicated times, and stained for phospho-Y783 of PLCγ1 (A) or phospho-Y319 of Zap70 (C). Intensity of antibody staining is pseudocolored. Cont, control. Bars, 5 µm. (B and D) Analysis of fluorescence intensities from phospho-PLCγ1 (A) or phospho-Zap70 (C) staining. The IS outlines were gauged by F-actin intensity; total phosphoprotein intensity per IS was calculated for a mean of 45 cells (B) or 35 cells (D) per condition. Mean ± SEM is shown. *, $P < 0.05$; ***, $P < 0.001$.

thapsigargin (Tg) to pharmacologically empty ER stores. In both cases, Tg treatment restored intracellular Ca^{2+} to normal levels, indicating that CRAC activity is intact. Collectively, these data show that F-actin retrograde flow maintains sustained Ca^{2+} signaling by regulating Ca^{2+} release from ER stores.

F-actin retrograde flow maintains activation of PLCγ1 in MCs

Ca^{2+} store release is regulated by signaling through PLCγ1-dependent cleavage of PIP_2 to generate IP_3, which stimulates receptors in the ER membrane (Zhang et al., 1999). To ask whether PLCγ1 activation is intact in T cells under conditions in which F-actin dynamics have been perturbed, cells were incubated in the presence or absence of Y-27632 and allowed to spread on OKT3-coated surfaces. After 5 min, cells were treated with vehicle alone or with JAS to freeze the actin network. Cells were fixed at either early times of treatment (5 min + 2 min) or late times (5 min + 10 min) and labeled for PLCγ1 phosphorylated at Y783, which represents the active enzyme pool (Kim et al., 1991). Control T cells formed numerous MCs containing phospho-PLCγ1, and these became more prevalent within the central regions of the IS at later time points (Fig. 7 A). Treatment of cells with Y-27632 alone had little effect on the intensity of phospho-PLCγ1 staining or on the distribution of phospho-PLCγ1 MCs, consistent with our finding that Ca^{2+} signaling is intact in these cells. In contrast, treatment with Y-27632 together with JAS resulted in a loss of phospho-PLCγ1 signal at the IS. Loss of phospho-PLCγ1 intensity was detectable by 2 min after JAS treatment and further decreased over time; by 10 min, the phospho-PLCγ1 signal was only 59% of control (Fig. 7 B). Interestingly, loss of F-actin dynamics did not affect phosphorylation of Zap70 on Y319 (Fig. 7, C and D). Furthermore, SLP-76 phosphorylation at positions Y128 or Y145 showed no dependence on myosin IIA or F-actin dynamics (Fig. S4). These results indicate that F-actin dynamics selectively sustain IS-associated PLCγ1 activation, leading to sustained Ca^{2+} signaling.

Discussion

The central role of the actin cytoskeleton in T cell activation was recognized in the 1980s, but exactly how actin orchestrates T cell signaling has remained enigmatic. Early studies relying on actin depolymerizing agents could demonstrate a requirement for actin but could not define whether actin functions as a static scaffold or whether dynamic processes such as turnover and motility were involved (Campi et al., 2005; Varma et al., 2006). More recent work has successfully addressed the role of individual actin regulatory proteins (Burkhardt et al., 2008), but this approach does not provide a sense of the coordinated behavior of the cytoskeletal network. Here, we took a pharmacological approach to systematically study the roles of actin polymerization and myosin II contractility in controlling protein dynamics and signaling at the IS. Our findings demonstrate that the actomyosin

network is a complex functional unit, with retrograde flow driven primarily by actin polymerization and organizing contractile forces provided by myosin II. We show that ongoing actin polymerization is required for centralization of signaling MCs and for tyrosine phosphorylation events leading to sustained Ca^{2+} signaling.

The actomyosin network in spreading T cells exhibits an actin-rich periphery, an actomyosin-rich ring, and a central actomyosin–poor region corresponding to the LP, LM, and CB regions of other cell types (Cai et al., 2006). In particular, IS cytoarchitecture bears a striking resemblance to that of fish keratocytes (Yam et al., 2007), cells used as a model of protrusion-based motility. In keratocytes, as in T cells, actin retrograde flow is very fast (40–100 vs. 5–8 nm/s in some epithelial cells; Ponti et al., 2004). Our estimates of actin retrograde flow rates within the LP are in good agreement with values in the literature (Nguyen et al., 2008; Yu et al., 2010). However, we find that actin flow slows with movement toward the CB. This behavior has been has been previously noted in T cells (Yu et al., 2010) and is also observed in keratocytes (Yam et al., 2007). Based on a study pioneered in keratocytes (Wilson et al., 2010), we used a panel of pharmacological inhibitors to dissect the roles of actin polymerization and myosin contractility in driving overall flow of the T cell actomyosin network. We show that actin polymerization generates most of the force in this system. Previous work shows that this polymerization is performed by the Arp2/3 complex in response to activation by WAVE2, HS1, and Wiskott–Aldrich syndrome protein (Gomez et al., 2006, 2007; Nolz et al., 2006). Although we did not find a role for myosin IIA in driving F-actin flow, we did find that myosin activity maintains the radial symmetry and overall organization of the IS, presumably by cross-linking antiparallel actin filaments and creating a meshed network that functions as a synchronous unit. Moreover, as in nonhematopoietic cells (Cai et al., 2006), myosin IIA activity limits T cell spreading and promotes a contraction phase during IS maturation. This contraction phase is similar to, albeit more modest than, the response in B cells during antigen gathering (Schnyder et al., 2011). Interestingly, Jurkat T cells also express myosin IIB (Fig. S2 B; Jbireal et al., 2010). Residual contraction was observed in cells suppressed for myosin IIA and treated with JAS, suggesting that myosin IIB contributes to contractile forces in these cells.

Quantitative comparison of F-actin and SLP-76 MC velocities yielded surprising results. Within the LP region, we found that SLP-76 MC centralization was slower than actin retrograde flow by a factor of ∼0.7. This effect was reported previously by Nguyen et al. (2008) and was interpreted as a duty ratio, representing intermittent attachment/detachment of MCs to the continuously moving F-actin network. Similar observations were reported for integrin and TCR MCs, where the duty ratio with actin was ∼0.4 (Kaizuka et al., 2007). Strikingly, however, we show that although actin flow slows with centripetal movement, SLP-76 MCs exhibit relatively uniform velocity and ultimately outpace the actomyosin network. We conclude that actin retrograde flow cannot be the sole driver of MC centrali zation and that other forces must be at play. It seems likely that microtubules are involved, as recent studies show that cytoplasmic dynein drives TCR MC movement into the cSMAC (Hashimoto-Tane et al., 2011). Although a handoff from actin in the IS periphery to microtubules in the IS center could be envisioned, there is evidence for a more complex mechanism. First, MCs do not collapse onto the microtubule-organizing center after F-actin depolymerization (Varma et al., 2006; Nguyen et al., 2008). Second, we find that virtually all MC movement is arrested under conditions that freeze actin flow, even within the actin-poor cSMAC region. These findings and studies showing alteration of the microtubule network in response to perturbation of actin binding proteins such as ezrin (Lasserre et al., 2010) point to intimate cross-talk between the F-actin and microtubule networks and to simultaneous interaction of MCs with both networks (Lasserre and Alcover, 2010).

The pharmacological approach used here sheds new light on the role of actin scaffolding, actin turnover, and myosin contractility on specific aspects of T cell signaling. The requirement for myosin II in TCR signaling has been debated. Jacobelli et al. (2004) found that myosin IIA suppression or inhibition in mouse primary T cells (which express only myosin IIA) affected T cell polarity and migration but not IS formation. However, Ilani et al. (2009) reported that inhibition of myosin II or suppression of myosin IIA heavy chain diminished tyrosine phosphorylation and ablated Ca^{2+} signaling. In our hands, myosin II activity was not needed for cell spreading or F-actin retrograde flow in Jurkat or human primary T cells. Moreover, in Jurkat T cells, we found that myosin II inhibition did not affect MC centralization, tyrosine phosphorylation, or Ca^{2+} flux. The explanation for these conflicting results is not clear but may involve differences in experimental approaches. In particular, whereas we used glass coverslips coated with immobilized anti-CD3, Ilani et al. (2009) used supported lipid bilayers coated with anti-CD3 and ICAM-1. It will be interesting to assess whether the requirement for myosin IIA depends on ligand mobility or on integrin-mediated adhesion, which is necessary for spreading on bilayers (Grakoui et al., 1999).

After this manuscript was submitted for review, Yi et al. (2012) published a closely related study describing the actomyosin network in Jurkat T cells. Our findings support and extend those of Yi et al. (2012), and the areas in which our results differ are informative. We observed lamellipodial, lamellar, and actin-poor regions of the IS, which is in excellent agreement with the regions described by Yi et al. (2012). Two comparatively minor differences exist between the two studies with respect to cytoarchitecture. First, Yi et al. (2012) emphasize the presence of actomyosin arcs within the lamellar region. We, too, observe these structures, although in our hands, they are rarely obvious and only become prominent in cells expressing high levels of F-tractin or labeled myosin IIA. Second, Yi et al. (2012) reported a sharp LP/LM boundary, like that found in tightly adherent migrating cells (Ponti et al., 2004); however, we have analyzed retrograde flow rates with 1–2-µm resolution across this region and find that actin deceleration is a linear function of IS radius. Moreover, we observe that actin speckles traverse this boundary. Thus, we conclude that actin flow at the LP/LM boundary undergoes

a gradual transition similar to that found in loosely adherent cells such as keratocytes (Yam et al., 2007). Another area in which our results differ from those of Yi et al. (2012) concerns the contribution of myosin II to driving actin retrograde flow. Both studies show that actin polymerization provides a large component of the force driving retrograde flow of the actomyosin network, whereas myosin contraction imposes radial organization on the network. However, we observed no effect of myosin II inhibition or suppression on actin retrograde flow, whereas Yi et al. (2012) show slowing of the actin network in blebbistatin-treated cells. This difference may be a result of the stimulatory surfaces used (immobilized anti-CD3 vs. mobile anti-CD3 and ICAM-1).

Probably the most informative difference between our work and Yi et al. (2012) involves the relationship of the actomyosin network to MC movement. In both cases, arresting actomyosin flow with a combination of inhibitors arrests centripetal MC movement. However, under steady-state conditions, Yi et al. (2012) show that centripetal movement TCR MCs track with F-actin flow, whereas we observed a striking disconnect between the rates of SLP-76 MC movement and actin flow. This is almost certainly a result of differences in the proteins under investigation. SLP-76 MCs are known to be mobile under conditions in which TCR MCs are not, and we recently showed in collaboration with the Baumgart laboratory that the velocity of ZAP-70 MCs (which presumably report on TCR localization) is affected by altered ligand mobility, whereas SLP-76 MCs are independent of this variable (Hsu et al., 2012). As previously discussed, both types of MCs are likely to interact with both the actin and microtubule cytoskeletons, but these data point to fundamental differences in the nature or extent of these interactions.

Whereas Yi et al. (2012) focused on describing actomyosin dynamics, we took advantage of our ability to manipulate those dynamics to probe T cell signaling under conditions that freeze actomyosin flow but leave the network intact. This is a powerful technique, as it allows us to ask for the first time whether the presence of an actin scaffold is sufficient to support signaling or whether actin turnover and flow are required. Our results clearly show that ongoing actin dynamics are required to sustain TCR signaling. We observed a drop in intracellular Ca^{2+} almost immediately after F-actin polymerization was inhibited, regardless of whether the F-actin network was allowed to collapse inward or was immobilized by pretreatment with myosin inhibitors. The decrease in intracellular Ca^{2+} could be rescued by Tg treatment, indicating that CRAC channels operate normally under conditions in which actin turnover is blocked. This finding is consistent with work by Mueller et al. (2007), who showed that CRAC channels function independently of cortical actin in T cells. It is currently unclear how to reconcile these findings with our previous work showing that expression of WAVE2, a key actin nucleation–promoting factor, interferes with coupling of ER store release to CRAC channel opening (Nolz et al., 2006). One possibility is that the requirement for WAVE2 does not involve its actin polymerizing activity. The ability of Tg to rescue Ca^{2+} influx in actin-immobilized T cells points to a defect in Ca^{2+} release from ER stores. In keeping with this, we found diminished levels of phosphorylated PLCγ1 at the IS under conditions of actin immobilization. Phosphorylation of Zap70 and its substrate SLP-76, which lie upstream of PLCγ1 in the TCR signaling cascade, is intact, indicating that actin immobilization affects a specific PLCγ1-proximal signaling event, possibly involving its activating kinase Itk. In keeping with this idea, both Itk and PLCγ1 interact with actin, and we previously observed defects in PLCγ1 function in T cells deficient for the actin regulatory protein HS1 (Gomez et al., 2006; Carrizosa et al., 2009).

Our ability to freeze actomyosin flow is also informative with respect to the mechanobiology of MC signaling. Retention of MCs in the IS periphery induced by integrin engagement, genetic perturbations, or physical barriers correlates with enhanced T cell activation, and it has been proposed that this reflects the fact that active signaling takes place in peripheral MCs, whereas signal extinction takes place in the cSMAC (Mossman et al., 2005; Nguyen et al., 2008; Lasserre et al., 2010; Hashimoto-Tane et al., 2011). However, we find that MC arrest under actin freeze conditions is not sufficient to enhance signaling; on the contrary, signaling is lost under these conditions. Two models are compatible with our data. First, actin flow could promote signaling by generating tension on receptors or signaling complexes. Such tension would be released by inhibiting actin flow but enhanced by restraining ligand or MC movement. The TCR is a mechanosensor that interacts with the actin cytoskeleton (Kim et al., 2009; Li et al., 2010), and actin flow could induce conformational change in the TCR. Given our results showing phosphorylation defects downstream of Zap70, however, molecules such as Itk or PLCγ1 might be the relevant, tension-sensitive molecules. An alternative possibility is that signaling requires ongoing MC biogenesis. F-actin depletion blocks MC formation without perturbing older MCs and leads to loss of signaling (Campi et al., 2005; Varma et al., 2006). Similarly, interruption of TCR–peptide-MHC interactions prevents MC formation and induces loss of intracellular Ca^{2+} without affecting MC centralization (Varma et al., 2006). Our work extends these findings. Under our freeze condition, no new MCs are formed (Video 9), demonstrating that the presence of F-actin is not sufficient for MC formation; ongoing polymerization is required.

Models based on tension and on new MC formation are not mutually exclusive. Indeed, we hypothesize that the two processes are mechanistically linked. We propose that peripheral actin-rich sites nucleate assembly of signaling complexes, which are initially associated with both extracellular ligands and the flowing cytoskeleton. Tension-induced signaling would be maximal immediately before initiation of MC movement, and movement would partially relieve tension and dampen signaling. This model has significant physiological implications. For example, ligand mobility on the surface of APCs is predicted to be an important parameter for modulating T cell responses, and molecules that link signaling intermediates to the cytoskeletal network should be interesting therapeutic targets. Future studies will be directed at testing these predictions.

Materials and methods

Reagents and antibodies

Y-27632 and blebbistatin were obtained from EMD Chemicals. JAS, Alexa Fluor 594 phalloidin, fura-2 acetoxymethyl ester, and goat anti–mouse IgG Alexa Fluor 680 were purchased from Invitrogen. T cells were stimulated

with LEAF-purified CD3-ε antibody (OKT3; BioLegend). Poly-L-lysine was purchased from Sigma-Aldrich. Rabbit polyclonal antibodies against phospho-MLC (pS19), phospho-PLCγ1 (pY783), and phospho-Zap70 (pY319) and rabbit polyclonal antibody specific for myosin IIB heavy chain were obtained from Cell Signaling Technology. Rabbit polyclonal antibody against myosin IIA heavy chain was obtained from Covance, mouse anti–glyceraldehyde 3-phosphate dehydrogenase (GAPDH) was obtained from Millipore, and goat anti–rabbit IgG IRDye800 was obtained from Rockland Immunochemicals Inc. Anti-phospho–SLP-76 (pY145) was purchased from Epitomics, Inc., and Alexa Fluor 647 anti-phospho–SLP-76 (phospho-Y128) was purchased from BD.

Cell culture

Jurkat cells stably expressing GFP-actin (Gomez et al., 2006) were used, except where indicated. J14 (SLP-76 deficient) Jurkat cells stably reconstituted with GFP–SLP-76 (Baker et al., 2009) were obtained from G. Koretzky (University of Pennsylvania, Philadelphia, PA). Cells were cultured in RPMI-1640 containing 10% FBS, GlutaMAX, and penicillin/streptomycin (Invitrogen) at 37°C in 5% CO_2. Primary peripheral $CD4^+$ T cells were obtained from the University of Pennsylvania's Human Immunology Core Facility under an Institutional Review Board–approved protocol. T cells were cultured in a humidified 5% CO_2 atmosphere at 37°C using X-VIVO 15 medium (Lonza) supplemented with 5% human serum (GemCell), 10 mM Hepes, L-GlutaMAX, penicillin G, and streptomycin. T cell blasts were generated by mixing with 4.5-µm paramagnetic Dynabeads (Invitrogen) with surface-immobilized antibodies against human CD3 (clone OKT3) and human CD28 (clone 9.3) at a 3:1 bead/cell ratio, as previously described. 6 d after activation, the stimulatory beads were removed from T cell cultures by magnetic separation to permit reexpression of surface CD3 on the T cell blasts.

Plasmids, oligonucleotides, and transfection

A construct expressing a full-length NMHC II-A N-terminally tagged with EGFP (Wei and Adelstein, 2000) was obtained from Addgene. A plasmid encoding NMHC II-A tagged with mKate2 was constructed in our laboratory. 5′-tgcaggatcc*accggt*cgccaccATGGTGAGCGAGCTGATTAAGGAG-3′ and 5′-gccat*aagctt*ccggaacctcctccaccTCTGTGCCCCAG-3′ were used to PCR amplify mKate2 tag from the pmKate2–β actin vector (Evrogen); capital letters indicate the tag, and Age I and Hind III restriction sites are italicized. The PCR product was digested with Age I and Hind III and swapped with EGFP in the pEGFP–NMHC II-A–C3 plasmid. F-tractin (ITPKA-9-40) tagged with tdTomato was a gift from M. Schell (Uniformed Services University, Bethesda, MD; Johnson and Schell, 2009). Transient transfection of Jurkat T cells by electroporation was performed as in Carrizosa et al. (2009). 16 h after transfection, live cells were enriched using a Ficoll-Paque gradient and imaged as described in the Fluorescence microscopy section. For protein knockdown, ON-TARGETplus SMARTpool of siRNA duplexes against Myh9 and siGENOME nontargeting siRNA control #2 were purchased from Thermo Fisher Scientific. 500 pmol of oligonucleotides was used for transfection. 48 h after transfection, cells were used in live-cell imaging experiments, and protein knockdown was assessed by Western blotting.

Transfection of primary human T cells was performed using electroporation of in vitro transcribed mRNA. To prepare mRNA, the EGFP-actin fusion protein coding sequence was cloned 3′ to the T7 promoter of the pGEM-64A plasmid (provided by Y. Zhao, University of Pennsylvania, Philadelphia, PA; Zhao et al., 2006). In vitro transcription of 7-mG(ppp)G–capped and polyadenylated EGFP-actin mRNA was performed using the mScript mRNA kit (Epicentre) in accordance with the manufacturer's instructions. After purification, GFP-actin mRNA was evaluated for polyadenylation and overall RNA quality by electrophoresis using a 1% agarose gel and ethidium bromide staining. 5.0×10^6 $CD4^+$ T cell blasts were washed once with PBS and resuspended in 100 µl RPMI-1640 medium without additives. 10 µg of the in vitro transcribed EGFP-actin mRNA was added to the cell suspension, and the cell/mRNA mixture was transferred to a 2-mm cuvette (BTX). Electroporation with a single 500-V pulse of a 720-µs duration was performed using an ElectroSquarePorator ECM 830 (BTX). Electroporated cells were transferred to a culture flask containing 10 ml RPMI-1640 medium, 10% FBS (HyClone; Thermo Fisher Scientific), and 10 mM Hepes and incubated for 17–20 h before use.

Biochemical analysis of myosin II inhibition and expression

To verify Y-27632 activity, Jurkat T cells were pretreated for 15 min with DMSO alone or 25 µM Y-27632 and stimulated with soluble OKT3 (1 µg/ml) for 5 min. Cells were then washed in cold PBS and lysed at 4°C in 50 mM Tris-HCl, pH 7.5, 150 mM NaCl, 5 mM EDTA, 1% Triton X-100, 10 mM NaF, 1 mM Na_3VO_4, and protease inhibitors. For Western blotting, lysates were separated on a NuPAGE gel (Invitrogen), transferred to nitrocellulose, probed as indicated, and imaged on a fluorescence scanner (Odyssey; LI-COR Biosciences) within the linear range.

Fluorescence microscopy

For imaging of fixed cells, 12-mm coverslips were coated with poly-L-lysine, as previously described (Bunnell et al., 2003), followed by 10 µg/ml OKT3 (2 h at 37°C or overnight at 4°C) and washed with PBS. Cells were harvested and resuspended at 5×10^5/ml in L-15 medium (Invitrogen) with 2 mg/ml D-glucose. Coverslips were equilibrated at 37°C, and 1.0×10^5 cells were allowed to interact with the surface for the indicated times. Cells were fixed in 3% PFA and labeled as in Dehring et al. (2011). Cells were imaged on a microscope (Axiovert200; Carl Zeiss) equipped with a spinning-disk confocal system (UltraView ERS 6; PerkinElmer) and a 63× Plan-Apochromat 1.4 NA objective. Images were collected using an ORCA-ER camera (Hamamatsu Photonics) and analyzed using Volocity software (v5.5; PerkinElmer). Unless indicated, 1-µm-thick z stacks of three images were collected at the T cell–coverglass interface and displayed as extended projections.

For live-cell imaging, 8-well chambered coverglasses (Lab-Tek II; Thermo Fisher Scientific) were coated with OKT3, as described in the preceding paragraph. Immediately before imaging, wells were covered with 400 µl of imaging medium (phenol red–free RPMI-1640 and 25 µM Hepes) and equilibrated to 37°C on the microscope stage within an environmental chamber (Solent Scientific). Cells were harvested and resuspended in imaging medium at 2×10^6/ml, and 5–10 µl of cell suspension was added to the well. Time-lapse images were collected at 63× using the same microscope as described in the previous paragraph. 1-µm-thick z stacks of three images were collected every 3 s for 5–7 min. Emission discrimination filters were used for multicolor imaging. 20–40 randomly selected cells were analyzed per condition.

Single-cell Ca^{2+} assays

Jurkat T cells were loaded with 3 µM fura-2 acetoxymethyl ester in RPMI for 15 min at 37°C, washed in L-15 medium supplemented with 2 mM $CaCl_2$, and resuspended at 2×10^6/ml. Cell were dropped on OKT3-coated and heated Delta T dishes (Bioptechs) and imaged every 3 s by sequential illumination with 340- and 380-nm lasers. Acquisition was performed on a microscope (DMI6000; Leica) using an ORCA-03G camera (Hamamatsu Photonics) and 40× oil objective, and images were analyzed with MetaFluor (Molecular Devices). For inhibitor studies, cells were pretreated with 25 µM Y-27632 concomitant with fura-2 incubation, washed in L-15 medium with Y-27632, and imaged in drug-containing medium. JAS or DMSO was added after the cells had reached a plateau in Ca^{2+} response (5 min into spreading). In some experiments, 1 µM Tg was added to block Ca^{2+} uptake into ER stores. Ca^{2+} mobilization was analyzed by plotting 340/380-nm ratios from individual cells over time. Averaged traces from multiple cells are shown.

Image analysis and statistical evaluation

Retrograde flow of the actin network was measured in two ways. First, videos of T cells expressing GFP-actin were processed using the Smart Sharpen filter in Photoshop (Adobe), with 300% amplification of local maxima within a 3-pixel radius. This facilitated identification of individual GFP-actin speckles, which were used as fiduciary marks for analysis. Analysis of sharpened and unprocessed videos yielded similar results, and images are shown without sharpening unless otherwise specified. Alternatively, a region of the F-actin network was photobleached to induce a synchronous wave of bleached GFP-actin propagating toward the center of the IS. In both cases, a ray was struck from the center of the IS to the periphery, and vertical kymographs were generated in Volocity (v5.5) and analyzed in ImageJ 1.45k (National Institutes of Health). Actin flow rate was calculated based on the angle of deflection from the vertical direction. Instantaneous velocities were plotted as a function of relative position along the IS radius.

SLP-76 MC tracking was performed using custom algorithms in Volocity and Excel (Microsoft). Objects with intensities 1.5 SD above the mean intensity of the IS were identified and filtered by size and then tracked using the Shortest Path algorithm in Volocity. Instantaneous velocities and (x, y) coordinates of each MC were exported into Excel, and the distance from the IS centroid was calculated for each MC at each time point. Instantaneous MC velocities within each 1-µm segment along the IS radius were averaged and plotted as a function of radius. Kymography was used to confirm the findings from particle tracking for individual MCs.

For this, maximum-over-time projections were generated from videos and used to define the tracks of MC movement. Kymographs were generated along these tracks, and MC velocity was calculated based on the angle of deflection from the vertical direction.

To measure the distribution of cytoskeletal components across the IS, a 0.5-µm-thick line was drawn along the diameter of spreading cells, and fluorescence intensity profiles were measured. To assess IS area and shape, custom algorithms in Volocity were used to identify cells based on intensity of the F-actin network. IS area was calculated automatically by integrating the pixels within the identified objects. IS shape (circularity) was calculated using the equation

$$S = \frac{P^2}{4\pi A},$$

where S represents IS shape and P and A are perimeter and area, respectively. To assess PLCγ1 activation, spreading GFP-actin–expressing cells were fixed and labeled with anti–phospho-PLCγ1, and cell boundaries were defined based on actin fluorescence intensity using a custom algorithm in Volocity. For each cell profile, background signal was subtracted, and total phospho-PLCγ1 signal intensity was quantified. Values from 80 cells were averaged for each experimental condition.

Statistical analysis was performed using Excel, with statistical significance determined using a two-tailed Student's *t* test for unpaired samples with unequal variances. Outliers were discounted as being 1.5 SD away from the mean. Representative images were selected within 0.5 SD from the mean.

Online supplemental material

Fig. S1 shows measurement of F-actin dynamics at the IS. Fig. S2 shows assessment of F-actin dynamics in response to JAS treatment of cells suppressed for myosin IIA. Fig. S3 shows measurement of SLP-76 MC velocities at the IS. Fig. S4 shows assessment of SLP-76 phosphorylation in response to F-actin immobilization. Video 1 shows myosin IIA and F-actin dynamics at the IS. Video 2 shows that F-actin features at the IS slow down toward the center of the IS. Video 3 shows photobleaching of GFP-actin, revealing F-actin velocity at the IS. Video 4 shows that actin and myosin IIA collapse to the center of the IS of Jurkat T cells upon stabilization of actin filaments. Video 5 shows that the F-actin network collapses to the center of the IS in human primary T cells upon stabilization of actin filaments. Video 6 shows that F-actin retrograde flow is unperturbed in cells pretreated with Y-27632. Video 7 shows that myosin II inhibition with blebbistatin does not affect actin retrograde flow (part A) and that myosin IIA suppression does not affect actin retrograde flow and leads to slow actin network collapse upon F-actin stabilization (part B). Video 8 shows that pretreatment with Y-27632 and acute treatment with JAS arrest F-actin retrograde flow in Jurkat T cells (part A) or in human primary T cells (part B). Video 9 shows that actin dynamics govern SLP-76 MC movement. Video 10 shows that SLP-76 MCs coalesce at the center of the IS. Online supplemental material is available at http://www.jcb.org/cgi/content/full/jcb.201201018/DC1.

The authors thank Dr. John Hammer, Jason Yi, Dr. Julie Theriot, William Comrie, Dr. Yair Argon, and Dr. Michael Lipscomb for helpful discussions.

This work was supported by National Institutes of Health grants R01AI065644 and P01CA093615 (to J.K. Burkhardt), PN2 EY016586 (to M.C. Milone), and 5T32AR7442-25 (to A. Babich).

The authors have no competing financial interests.

Submitted: 4 January 2012
Accepted: 8 May 2012

References

Alon, R., and M.L. Dustin. 2007. Force as a facilitator of integrin conformational changes during leukocyte arrest on blood vessels and antigen-presenting cells. *Immunity*. 26:17–27. http://dx.doi.org/10.1016/j.immuni.2007.01.002

Baker, R.G., C.J. Hsu, D. Lee, M.S. Jordan, J.S. Maltzman, D.A. Hammer, T. Baumgart, and G.A. Koretzky. 2009. The adapter protein SLP-76 mediates "outside-in" integrin signaling and function in T cells. *Mol. Cell. Biol.* 29:5578–5589. http://dx.doi.org/10.1128/MCB.00283-09

Beemiller, P., and M.F. Krummel. 2010. Mediation of T-cell activation by actin meshworks. *Cold Spring Harb. Perspect. Biol.* 2:a002444. http://dx.doi.org/10.1101/cshperspect.a002444

Bubb, M.R., A.M. Senderowicz, E.A. Sausville, K.L. Duncan, and E.D. Korn. 1994. Jasplakinolide, a cytotoxic natural product, induces actin polymerization and competitively inhibits the binding of phalloidin to F-actin. *J. Biol. Chem.* 269:14869–14871.

Bunnell, S.C., V. Kapoor, R.P. Trible, W. Zhang, and L.E. Samelson. 2001. Dynamic actin polymerization drives T cell receptor-induced spreading: A role for the signal transduction adaptor LAT. *Immunity*. 14:315–329. http://dx.doi.org/10.1016/S1074-7613(01)00112-1

Bunnell, S.C., D.I. Hong, J.R. Kardon, T. Yamazaki, C.J. McGlade, V.A. Barr, and L.E. Samelson. 2002. T cell receptor ligation induces the formation of dynamically regulated signaling assemblies. *J. Cell Biol.* 158:1263–1275. http://dx.doi.org/10.1083/jcb.200203043

Bunnell, S.C., V.A. Barr, C.L. Fuller, and L.E. Samelson. 2003. High-resolution multicolor imaging of dynamic signaling complexes in T cells stimulated by planar substrates. *Sci. STKE*. 2003:PL8. http://dx.doi.org/10.1126/stke.2003.177.pl8

Bunnell, S.C., A.L. Singer, D.I. Hong, B.H. Jacque, M.S. Jordan, M.C. Seminario, V.A. Barr, G.A. Koretzky, and L.E. Samelson. 2006. Persistence of cooperatively stabilized signaling clusters drives T-cell activation. *Mol. Cell. Biol.* 26:7155–7166. http://dx.doi.org/10.1128/MCB.00507-06

Burkhardt, J.K., E. Carrizosa, and M.H. Shaffer. 2008. The actin cytoskeleton in T cell activation. *Annu. Rev. Immunol.* 26:233–259. http://dx.doi.org/10.1146/annurev.immunol.26.021607.090347

Cai, Y., N. Biais, G. Giannone, M. Tanase, G. Jiang, J.M. Hofman, C.H. Wiggins, P. Silberzan, A. Buguin, B. Ladoux, and M.P. Sheetz. 2006. Nonmuscle myosin IIA-dependent force inhibits cell spreading and drives F-actin flow. *Biophys. J.* 91:3907–3920. http://dx.doi.org/10.1529/biophysj.106.084806

Campi, G., R. Varma, and M.L. Dustin. 2005. Actin and agonist MHC-peptide complex-dependent T cell receptor microclusters as scaffolds for signaling. *J. Exp. Med.* 202:1031–1036. http://dx.doi.org/10.1084/jem.20051182

Carrizosa, E., T.S. Gomez, C.M. Labno, D.A. Klos Dehring, X. Liu, B.D. Freedman, D.D. Billadeau, and J.K. Burkhardt. 2009. Hematopoietic lineage cell-specific protein 1 is recruited to the immunological synapse by IL-2-inducible T cell kinase and regulates phospholipase Cgamma1 Microcluster dynamics during T cell spreading. *J. Immunol.* 183:7352–7361. http://dx.doi.org/10.4049/jimmunol.0900973

Dehring, D.A., F. Clarke, B.G. Ricart, Y. Huang, T.S. Gomez, E.K. Williamson, D.A. Hammer, D.D. Billadeau, Y. Argon, and J.K. Burkhardt. 2011. Hematopoietic lineage cell-specific protein 1 functions in concert with the Wiskott-Aldrich syndrome protein to promote podosome array organization and chemotaxis in dendritic cells. *J. Immunol.* 186:4805–4818. http://dx.doi.org/10.4049/jimmunol.1003102

Gomez, T.S., S.D. McCarney, E. Carrizosa, C.M. Labno, E.O. Comiskey, J.C. Nolz, P. Zhu, B.D. Freedman, M.R. Clark, D.J. Rawlings, et al. 2006. HS1 functions as an essential actin-regulatory adaptor protein at the immune synapse. *Immunity*. 24:741–752. http://dx.doi.org/10.1016/j.immuni.2006.03.022

Gomez, T.S., K. Kumar, R.B. Medeiros, Y. Shimizu, P.J. Leibson, and D.D. Billadeau. 2007. Formins regulate the actin-related protein 2/3 complex-independent polarization of the centrosome to the immunological synapse. *Immunity*. 26:177–190. http://dx.doi.org/10.1016/j.immuni.2007.01.008

Grakoui, A., S.K. Bromley, C. Sumen, M.M. Davis, A.S. Shaw, P.M. Allen, and M.L. Dustin. 1999. The immunological synapse: A molecular machine controlling T cell activation. *Science*. 285:221–227. http://dx.doi.org/10.1126/science.285.5425.221

Hashimoto-Tane, A., T. Yokosuka, K. Sakata-Sogawa, M. Sakuma, C. Ishihara, M. Tokunaga, and T. Saito. 2011. Dynein-driven transport of T cell receptor microclusters regulates immune synapse formation and T cell activation. *Immunity*. 34:919–931. http://dx.doi.org/10.1016/j.immuni.2011.05.012

Houtman, J.C., Y. Higashimoto, N. Dimasi, S. Cho, H. Yamaguchi, B. Bowden, C. Regan, E.L. Malchiodi, R. Mariuzza, P. Schuck, et al. 2004. Binding specificity of multiprotein signaling complexes is determined by both cooperative interactions and affinity preferences. *Biochemistry*. 43:4170–4178. http://dx.doi.org/10.1021/bi0357311

Hsu, C.J., W.T. Hsieh, A. Waldman, F. Clarke, E.S. Huseby, J.K. Burkhardt, and T. Baumgart. 2012. Ligand mobility modulates immunological synapse formation and T cell activation. *PLoS ONE*. 7:e32398. http://dx.doi.org/10.1371/journal.pone.0032398

Ilani, T., G. Vasiliver-Shamis, S. Vardhana, A. Bretscher, and M.L. Dustin. 2009. T cell antigen receptor signaling and immunological synapse stability require myosin IIA. *Nat. Immunol.* 10:531–539. http://dx.doi.org/10.1038/ni.1723

Jacobelli, J., S.A. Chmura, D.B. Buxton, M.M. Davis, and M.F. Krummel. 2004. A single class II myosin modulates T cell motility and stopping, but not synapse formation. *Nat. Immunol.* 5:531–538. http://dx.doi.org/10.1038/ni1065

Jbireal, J.M., C. Strell, B. Niggemann, K. Zänker, and F. Entschladen. 2010. The selective role of myosin VI in lymphoid leukemia cell migration. *Leuk. Res.* 34:1656–1662. http://dx.doi.org/10.1016/j.leukres.2010.04.018

Johnson, H.W., and M.J. Schell. 2009. Neuronal IP3 3-kinase is an F-actin-bundling protein: Role in dendritic targeting and regulation of spine morphology. *Mol. Biol. Cell*. 20:5166–5180. http://dx.doi.org/10.1091/mbc.E09-01-0083

Kaizuka, Y., A.D. Douglass, R. Varma, M.L. Dustin, and R.D. Vale. 2007. Mechanisms for segregating T cell receptor and adhesion molecules during immunological synapse formation in Jurkat T cells. *Proc. Natl. Acad. Sci. USA*. 104:20296–20301. http://dx.doi.org/10.1073/pnas.0710258105

Kim, H.K., J.W. Kim, A. Zilberstein, B. Margolis, J.G. Kim, J. Schlessinger, and S.G. Rhee. 1991. PDGF stimulation of inositol phospholipid hydrolysis requires PLC-gamma 1 phosphorylation on tyrosine residues 783 and 1254. *Cell*. 65:435–441. http://dx.doi.org/10.1016/0092-8674(91)90461-7

Kim, S.T., K. Takeuchi, Z.Y. Sun, M. Touma, C.E. Castro, A. Fahmy, M.J. Lang, G. Wagner, and E.L. Reinherz. 2009. The alphabeta T cell receptor is an anisotropic mechanosensor. *J. Biol. Chem.* 284:31028–31037. http://dx.doi.org/10.1074/jbc.M109.052712

Lasserre, R., and A. Alcover. 2010. Cytoskeletal cross-talk in the control of T cell antigen receptor signaling. *FEBS Lett.* 584:4845–4850. http://dx.doi.org/10.1016/j.febslet.2010.09.001

Lasserre, R., S. Charrin, C. Cuche, A. Danckaert, M.I. Thoulouze, F. de Chaumont, T. Duong, N. Perrault, N. Varin-Blank, J.C. Olivo-Marin, et al. 2010. Ezrin tunes T-cell activation by controlling Dlg1 and microtubule positioning at the immunological synapse. *EMBO J.* 29:2301–2314. http://dx.doi.org/10.1038/emboj.2010.127

Lee, K.H., A.D. Holdorf, M.L. Dustin, A.C. Chan, P.M. Allen, and A.S. Shaw. 2002. T cell receptor signaling precedes immunological synapse formation. *Science*. 295:1539–1542. http://dx.doi.org/10.1126/science.1067710

Li, Y.C., B.M. Chen, P.C. Wu, T.L. Cheng, L.S. Kao, M.H. Tao, A. Lieber, and S.R. Roffler. 2010. Cutting Edge: Mechanical forces acting on T cells immobilized via the TCR complex can trigger TCR signaling. *J. Immunol.* 184:5959–5963. http://dx.doi.org/10.4049/jimmunol.0900775

Mossman, K.D., G. Campi, J.T. Groves, and M.L. Dustin. 2005. Altered TCR signaling from geometrically repatterned immunological synapses. *Science*. 310:1191–1193. http://dx.doi.org/10.1126/science.1119238

Mueller, P., A. Quintana, D. Griesemer, M. Hoth, and J. Pieters. 2007. Disruption of the cortical actin cytoskeleton does not affect store operated Ca2+ channels in human T-cells. *FEBS Lett.* 581:3557–3562. http://dx.doi.org/10.1016/j.febslet.2007.06.068

Negulescu, P.A., N. Shastri, and M.D. Cahalan. 1994. Intracellular calcium dependence of gene expression in single T lymphocytes. *Proc. Natl. Acad. Sci. USA*. 91:2873–2877. http://dx.doi.org/10.1073/pnas.91.7.2873

Nguyen, K., N.R. Sylvain, and S.C. Bunnell. 2008. T cell costimulation via the integrin VLA-4 inhibits the actin-dependent centralization of signaling microclusters containing the adaptor SLP-76. *Immunity*. 28:810–821. http://dx.doi.org/10.1016/j.immuni.2008.04.019

Nolz, J.C., T.S. Gomez, P. Zhu, S. Li, R.B. Medeiros, Y. Shimizu, J.K. Burkhardt, B.D. Freedman, and D.D. Billadeau. 2006. The WAVE2 complex regulates actin cytoskeletal reorganization and CRAC-mediated calcium entry during T cell activation. *Curr. Biol.* 16:24–34. http://dx.doi.org/10.1016/j.cub.2005.11.036

Oh-hora, M. 2009. Calcium signaling in the development and function of T-lineage cells. *Immunol. Rev.* 231:210–224. http://dx.doi.org/10.1111/j.1600-065X.2009.00819.x

Pollard, T.D., and J. Berro. 2009. Mathematical models and simulations of cellular processes based on actin filaments. *J. Biol. Chem.* 284:5433–5437. http://dx.doi.org/10.1074/jbc.R800043200

Ponti, A., M. Machacek, S.L. Gupton, C.M. Waterman-Storer, and G. Danuser. 2004. Two distinct actin networks drive the protrusion of migrating cells. *Science*. 305:1782–1786. http://dx.doi.org/10.1126/science.1100533

Schnyder, T., A. Castello, C. Feest, N.E. Harwood, T. Oellerich, H. Urlaub, M. Engelke, J. Wienands, A. Bruckbauer, and F.D. Batista. 2011. B cell receptor-mediated antigen gathering requires ubiquitin ligase Cbl and adaptors Grb2 and Dok-3 to recruit dynein to the signaling microcluster. *Immunity*. 34:905–918. http://dx.doi.org/10.1016/j.immuni.2011.06.001

Sherman, E., V. Barr, S. Manley, G. Patterson, L. Balagopalan, I. Akpan, C.K. Regan, R.K. Merrill, C.L. Sommers, J. Lippincott-Schwartz, and L.E. Samelson. 2011. Functional nanoscale organization of signaling molecules downstream of the T cell antigen receptor. *Immunity*. 35:705–720. http://dx.doi.org/10.1016/j.immuni.2011.10.004

Straight, A.F., A. Cheung, J. Limouze, I. Chen, N.J. Westwood, J.R. Sellers, and T.J. Mitchison. 2003. Dissecting temporal and spatial control of cytokinesis with a myosin II Inhibitor. *Science*. 299:1743–1747. http://dx.doi.org/10.1126/science.1081412

Ueda, K., M. Murata-Hori, M. Tatsuka, and H. Hosoya. 2002. Rho-kinase contributes to diphosphorylation of myosin II regulatory light chain in nonmuscle cells. *Oncogene*. 21:5852–5860. http://dx.doi.org/10.1038/sj.onc.1205747

Valitutti, S., D. Coombs, and L. Dupré. 2010. The space and time frames of T cell activation at the immunological synapse. *FEBS Lett.* 584:4851–4857. http://dx.doi.org/10.1016/j.febslet.2010.10.010

Varma, R., G. Campi, T. Yokosuka, T. Saito, and M.L. Dustin. 2006. T cell receptor-proximal signals are sustained in peripheral microclusters and terminated in the central supramolecular activation cluster. *Immunity*. 25:117–127. http://dx.doi.org/10.1016/j.immuni.2006.04.010

Wei, Q., and R.S. Adelstein. 2000. Conditional expression of a truncated fragment of nonmuscle myosin II-A alters cell shape but not cytokinesis in HeLa cells. *Mol. Biol. Cell*. 11:3617–3627.

Wilson, C.A., M.A. Tsuchida, G.M. Allen, E.L. Barnhart, K.T. Applegate, P.T. Yam, L. Ji, K. Keren, G. Danuser, and J.A. Theriot. 2010. Myosin II contributes to cell-scale actin network treadmilling through network disassembly. *Nature*. 465:373–377. http://dx.doi.org/10.1038/nature08994

Wülfing, C., and M.M. Davis. 1998. A receptor/cytoskeletal movement triggered by costimulation during T cell activation. *Science*. 282:2266–2269. http://dx.doi.org/10.1126/science.282.5397.2266

Yam, P.T., C.A. Wilson, L. Ji, B. Hebert, E.L. Barnhart, N.A. Dye, P.W. Wiseman, G. Danuser, and J.A. Theriot. 2007. Actin–myosin network reorganization breaks symmetry at the cell rear to spontaneously initiate polarized cell motility. *J. Cell Biol.* 178:1207–1221. http://dx.doi.org/10.1083/jcb.200706012

Yi, J., X.S. Wu, T. Crites, and J.A. Hammer III. 2012. Actin retrograde flow and actomyosin II arc contraction drive receptor cluster dynamics at the immunological synapse in Jurkat T cells. *Mol. Biol. Cell*. 23:834–852. http://dx.doi.org/10.1091/mbc.E11-08-0731

Yokosuka, T., K. Sakata-Sogawa, W. Kobayashi, M. Hiroshima, A. Hashimoto-Tane, M. Tokunaga, M.L. Dustin, and T. Saito. 2005. Newly generated T cell receptor microclusters initiate and sustain T cell activation by recruitment of Zap70 and SLP-76. *Nat. Immunol.* 6:1253–1262. http://dx.doi.org/10.1038/ni1272

Yu, C.H., H.J. Wu, Y. Kaizuka, R.D. Vale, and J.T. Groves. 2010. Altered actin centripetal retrograde flow in physically restricted immunological synapses. *PLoS ONE*. 5:e11878. http://dx.doi.org/10.1371/journal.pone.0011878

Zhang, J., A. Shehabeldin, L.A. da Cruz, J. Butler, A.K. Somani, M. McGavin, I. Kozieradzki, A.O. dos Santos, A. Nagy, S. Grinstein, et al. 1999. Antigen receptor-induced activation and cytoskeletal rearrangement are impaired in Wiskott-Aldrich syndrome protein-deficient lymphocytes. *J. Exp. Med.* 190:1329–1342. http://dx.doi.org/10.1084/jem.190.9.1329

Zhao, Y., Z. Zheng, C.J. Cohen, L. Gattinoni, D.C. Palmer, N.P. Restifo, S.A. Rosenberg, and R.A. Morgan. 2006. High-efficiency transfection of primary human and mouse T lymphocytes using RNA electroporation. *Mol. Ther.* 13:151–159. http://dx.doi.org/10.1016/j.ymthe.2005.07.688